





Impact of Leakage for Electricity Generation by Pyroelectric Converter

Chenbo Zhang (张晨波)^{1,2}, Zhuohui Zeng (曾卓晖)¹, Zeyuan Zhu (朱泽远)¹, Mostafa Karami,¹
and Xian Chen (陈弦)^{1,*}

¹*Department of Mechanical and Aerospace Engineering, Hong Kong University of Science and Technology, Clear Water Bay, Hong Kong*

²*HKUST Jockey Club Institute for Advanced Study, Hong Kong University of Science and Technology, Clear Water Bay, Hong Kong*

 (Received 15 September 2020; revised 16 November 2020; accepted 14 December 2020; published 31 December 2020)

Pyroelectric energy converters are functional capacitors that use a pyroelectric material as the dielectric layer. By utilizing a first-order phase transformation of the material, a pyroelectric device can generate an adequate amount of electricity from small temperature fluctuations. However, most pyroelectric capacitors leak during energy conversion. In this paper, we analyze the thermodynamics of pyroelectric energy conversion with consideration of electric leakage. Our thermodynamic model is verified by experiments using three phase-transforming ferroelectric materials with different pyroelectric properties and leakage behaviors. We demonstrate that the impact of leakage on electric generation is prominent, and sometimes may be confused with the actual power generation by pyroelectricity. We discover a material candidate, $(\text{Ba, Ca})(\text{Ti, Zr, Ce})\text{O}_3$, that exhibits a large pyroelectric current and an extremely low leakage current. A pyroelectric converter made of this material generates a pyroelectric current density of $1.95 \mu\text{A}/\text{cm}^2$ and a pyroelectric work density of $0.2 \text{ J}/\text{cm}^3$ even after 1389 thermodynamic-conversion cycles.

DOI: [10.1103/PhysRevApplied.14.064079](https://doi.org/10.1103/PhysRevApplied.14.064079)

I. INTRODUCTION

Energy harvesting from waste heat is an emerging research field in sustainable-energy science [1]. This heat, particularly in the low-grade regime (i.e., below 250°C), is abundant in nature and can be obtained from solar radiation and geothermal activity. Industry and human daily activities generate an immense amount of waste heat below 200°C . Ferroelectric materials with a temperature-dependent polarization have attracted increasing attention in recent years for electricity generation from temperatures from 40 to 150°C [2–5]. The mechanism of this energy conversion is commonly characterized as a pyroelectric effect. Many reported energy converters are made from a capacitor with a dielectric layer whose pyroelectric properties are designed for harvesting low-grade heat. Most of them are thin-film devices [4,5] working under a bias electric field, provided by external power. The electric energy generated by these devices is usually confused with the applied bias electric field. Without such a bias electric field, the performance of the energy conversion becomes rather marginal [2,4].

Removal of the bias electric field redefines the thermodynamic cycle for pyroelectric energy conversion based on small temperature fluctuations. Several thermodynamic models, depending on the initial conditions, have been

proposed for analyzing the power output of power-source-free pyroelectric generators [6–8]. In our previous study of phase-transformation pyroelectric energy conversion, the initial state of the thermodynamic system is chosen as (P_L, E_L, T_L) , where the temperature T_L is lower than the transition temperature, the working conjugate of the polarization is P_L , and the electric field is $E_L > 0$ in the ferroelectric phase. The initial polarization is achieved by use of an external dc voltage source. For a bulk capacitor with a thickness between 0.5 and 1 mm, the applied dc voltage is usually in the range of 30 – 50 V [6,7]. When the ferroelectric capacitor is balanced with its charge reservoir, the external dc voltage source is removed and the system is assumed to be electrically isolated. When the ferroelectric material undergoes a phase transformation, the charge starts flowing. Therefore, this is a constant-current-output energy-conversion device. Ideally, the total charge in the isolated system is preserved, if the phase-transforming dielectric layer is a perfect insulator. However, charge leakage is unavoidable and non-negligible, especially at elevated temperature, for perovskite oxides [8–13]. Over numerous energy-conversion cycles, the performance of the device degrades significantly, which greatly hinders the practical application of this energy-conversion technology. For thin-film capacitors, the leakage current is a more critical problem for electricity generation [10,13,14].

This paper theorizes about the impact of leakage on the power-source-free energy-conversion system shown

*xianchen@ust.hk

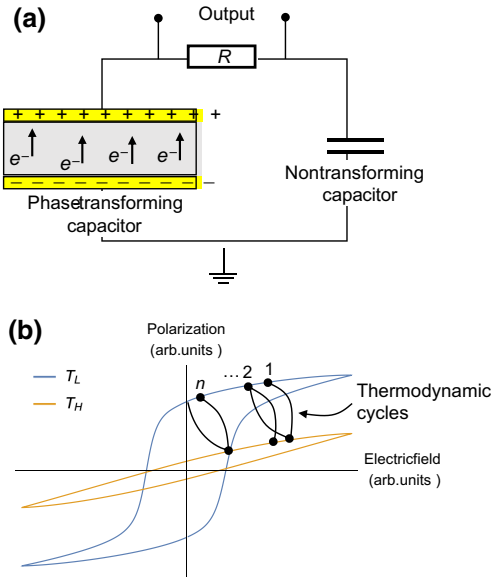


FIG. 1. (a) Schematic illustration of an energy-conversion system using a phase-transforming capacitor; (b) schematic illustration of polarization versus electric field for the ferroelectric (T_L) and paraelectric (T_H) phases, by means of which power-source-free thermodynamic cycles [6] are designed with consideration of the leakage-induced degradation.

in Fig. 1(a). The charge leaks inside the dielectric layer as the energy conversion begins. Unlike the case for an ideal insulation system, the electric field in the phase-transforming planar capacitor cannot reach its initial value again after each of the energy-conversion cycles, as illustrated in Fig. 1(b).

II. THERMODYNAMIC ANALYSIS

We consider the phase-transforming capacitor as a thermodynamic system. When the system fluctuates thermally about the phase-transformation temperature T_c , the charge Q held by the capacitor falls and rises accordingly due to the alternation of the capacitance caused by the first-order phase transformation between the ferroelectric and paraelectric phases. The charge can be expressed as a function of the temperature of the phase-transforming capacitor, T , and the voltage on the capacitor, V , i.e., $Q = Q(V, T)$. During the cyclic thermodynamic processes between the states (Q_L, V_L, T_L) and (Q_H, V_H, T_H) , where $T_L < T_c < T_H$, all three state variables (Q, V, T) change simultaneously without the application of a bias electric field [6]. If we consider a planar capacitor, the voltage is proportional to the electric field in the capacitor. Let $t = 0$ mark the time of the beginning of the first thermodynamic cycle [cycle 1 in Fig. 1(b)]. The electric field in the capacitor is

$$E(0) = E_0 = \frac{V_0}{d},$$

where V_0 is gained by connecting the whole electric circuit in Fig. 1(a) to an external dc source. Let $t > 0$ mark the time period of the energy-conversion processes after the removal of the external dc source. Because of electric leakage, the stored charge $Q(V, T)$ cannot reach the initial state of the previous thermodynamic cycle, as shown in Fig. 1(b). In this case, the relative starting state of the next cycle drifts down along the polarization curve. As a result, the thermodynamic system is cycle-dependent. Let the time t_n label the starting state of the n th cycle:

$$E(t_{n+1}) < E(t_n) < E(t_{n-1}) < \dots < E_0.$$

Consequently, the stored charge in the ferroelectric phase decreases after every cycle. If such leakage continues, there is no charge left after a finite number of energy-conversion cycles, which causes the electricity-generation process to cease.

A. Governing equations of energy conversion

At $t = 0$, the total charge in the system is calculated from

$$Q_{\text{tot}} = C_{\text{ref}}V_0 + Q(V_0, T_L), \quad (1)$$

where C_{ref} denotes the capacitance of the nontransforming capacitor, considered as a reference capacitor in our experiment. At $t > 0$, the charge balance can be expressed as

$$Q_{\text{tot}} - \int_0^t I_c(\xi) d\xi = Q_{\text{ref}}(t) + Q(V(t), T(t)), \quad (2)$$

where Q_{ref} is a time-dependent function defining the charge held by the reference capacitor for $t > 0$, and the function I_c represents the charge-leakage current in the phase-transforming ferroelectric capacitor, which is nonzero after energy conversion starts.

Considering the electric circuit in Fig. 1(a), we have

$$V(t) = V_d(t) + \frac{Q_{\text{ref}}(t)}{C_{\text{ref}}}, \quad (3)$$

where V_d is the voltage on the load resistor. Substituting Eq. (3) into Eq. (2) and taking the first-order time derivative, we get

$$\dot{Q} + C_{\text{ref}}\dot{V} + I_c - \dot{V}_d C_{\text{ref}} = 0. \quad (4)$$

Since Q is a function of V , Eq. (4) is a first-order ordinary differential equation (ODE) for the variables V and V_d . The voltage on the load resistor is attributed to the generation

of a current $-\dot{Q}$ and the leakage current I_c , as follows:

$$V_d = -(\dot{Q} + I_c)R. \quad (5)$$

Therefore, the governing equation can be written as

$$RC_{\text{ref}}\ddot{Q} + \dot{Q} + C_{\text{ref}}\dot{V} + I_c + RC_{\text{ref}}\dot{I}_c = 0. \quad (6)$$

Equation (6) is a second-order ODE for the variable V . We assume that the voltage applied across the thin-plate phase-transforming pyroelectric capacitor is linearly related to the electric field E by $V = Ed$, where d denotes the thickness of the thin plate. The constitutive relations for Q and I_c can be also characterized as $Q(E, T) = Aq(E, T)$ and $I_c(E, T) = AJ(E, T)$, where A is the area of the planar capacitor, and $q(E, T)$ and $J(E, T)$ are the charge density and leakage-current density. Modulated by the area A , Eq. (6) becomes

$$RC_{\text{ref}}\ddot{q} + \dot{q} + \frac{d}{A}C_{\text{ref}}\dot{E} + J + RC_{\text{ref}}\dot{J} = 0. \quad (7)$$

B. Characterization of ferroelectric properties

According to the constitutive relation [15], the charge density of the phase-transforming pyroelectric capacitor is a function of the electric field E and the temperature T ,

$$q = \varepsilon_0 E + P(E, T), \quad (8)$$

where ε_0 is the vacuum permittivity, and the constitutive function $P(E, T)$ is the polarization of the phase-transforming ferroelectric material. The first- and second-order time derivatives can be calculated directly from Eq. (8) using the partial differential quantities $P_{,E} = \partial P / \partial E$, $P_{,T} = \partial P / \partial T$, $P_{,EE} = \partial^2 P / \partial E^2$, $P_{,TT} = \partial^2 P / \partial T^2$, and $P_{,TE} = \partial^2 P / \partial T \partial E$, among which $\kappa = P_{,T}$ is an important ferroelectric property and is defined as the pyroelectric coefficient. This coefficient has been widely used to judge the performance of pyroelectric generators [3,5,16]. Note that when a first-order phase transformation is coupled with the pyroelectric properties, these derivatives vary with the temperature and electric field.

The constitutive relations $P(E, T)$ and $J(E, T)$ are experimentally characterized with a ferroelectric-analyzer system (aixACCT TF Analyzer 2000E). Figures 2(a) and 2(b) show the temperature-dependent ferroelectric polarization and leakage-current density in polycrystalline BaTiO₃ (BTO) under different electric fields from 0 to 2 kV/cm. At room temperature under a small applied field, the leakage-current density is about 0.1 $\mu\text{A}/\text{cm}^2$. The electric leakage of the material becomes more prominent at elevated temperatures under a larger applied electric field. In our energy-conversion experiment, the working electric field in the pyroelectric capacitor is between 0.5 and 1.2 kV/cm. When the applied electric field is higher than

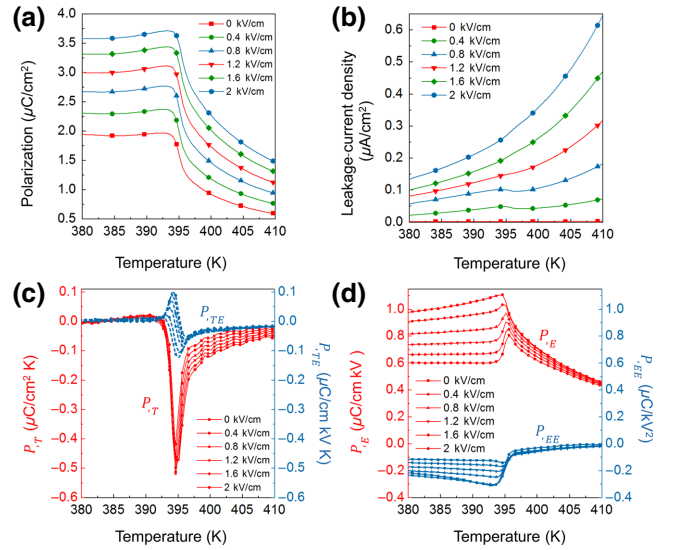


FIG. 2. Temperature-dependent (a) polarization and (b) leakage-current density of phase-transforming BaTiO₃ under electric fields from 0 to 2 kV/cm in the temperature range from 380 to 410 K, corresponding to the derivatives (c) $P_{,T}$ (red), $P_{,TE}$ (blue) and (d) $P_{,EE}$ (red), $P_{,EE}$ (blue).

1.2 kV/cm, the increase in the leakage current becomes much rapid in the elevated-temperature regime. In a thin-film capacitor, the leakage is more problematic than in the bulk. For example, the leakage current of a barium titanate thin-film capacitor is about 5–10 times larger under similar electric and thermal conditions [17]. Compared with barium titanate, PbTiO₃-based thin-film capacitors exhibit even larger leakage [17,18]. In the temperature regime characterized, the polarization of the material decreases as the temperature increases, with an abrupt drop at 395 K, which reveals the first-order phase transformation between the tetragonal and cubic phases. Evidently, Fig. 2(c) shows a singularity in the pyroelectric coefficient (i.e., $P_{,T}$) at 395 K. Similarly, the derivative $P_{,E}$ is also singular at the phase-transformation temperature. Because of this singularity, the conventional formula for the pyroelectric current [16] cannot be applied in the vicinity of the first-order phase transformation when a first-order phase transformation occurs. Instead, the Clausius-Clapeyron relation needs to be considered in a thermodynamic analysis of the energy-conversion process [6–8]. The second-order derivatives $P_{,EE}$ and $P_{,TE}$ are calculated numerically, as shown in Figs. 2(c) and 2(d), and are very small compared with the first-derivative functions. For simplicity, we neglect these second-order derivatives in the numerical solution of the governing equation (7). Note that we keep the second-order derivative $P_{,TT}$ in all computations.

After dropping terms $P_{,TE}$ and $P_{,EE}$, the governing equation (7) becomes

$$(\varepsilon_0 + P_{,E})\ddot{E} + C_1\dot{E} + C_2 = 0, \quad (9)$$

where

$$C_1 = \frac{1}{RC_{\text{ref}}}(\varepsilon_0 + P_{,E}) + \frac{d}{AR} + J_{,E}, \quad (10)$$

$$C_2 = P_{,T}\ddot{T} + P_{,TT}\dot{T}^2 + \left(\frac{P_{,T}}{RC_{\text{ref}}} + J_{,T}\right)\dot{T} + \frac{J}{RC_{\text{ref}}}. \quad (11)$$

This can be solved numerically for the initial conditions

$$E(0) = E_0 = \frac{V_0}{d}, \quad \dot{E}(0) = 0. \quad (12)$$

In order to benchmark materials of different geometry in various experimental settings, dimensionless variables are used in the governing equation; these are represented by symbols with an overbar, $\bar{\cdot}$. For a specific phase-transforming pyroelectric planar capacitor with thickness d and an initial charging voltage $V(0) = V_0$ associated with an electric field $E_0 = V_0/d$ at a temperature T_L lower than the phase transition temperature, the nondimensional voltage, electric field, temperature, and time are defined as

$$\bar{V} = \frac{V}{V_0}, \quad \bar{E} = \frac{E}{E_0}, \quad \bar{T} = \frac{T - T_L}{T_H - T_L}, \quad \bar{t} = \frac{t}{\tau}, \quad (13)$$

where the working temperature range of the device is between T_L and T_H , such that $T_L < T_c < T_H$. The process takes τ seconds per cycle, which fully covers the duration of the phase transformation. According to Eq. (13), the values of \bar{V} , \bar{E} , \bar{T} , and \bar{t} are all between 0 and 1. Let $P_L = P(E_0, T_L)$ be the initial polarization in the ferroelectric phase, and let $J_H = J(E_0, T_H)$ be the highest leakage-current density. The nondimensional polarization and leakage-current density are defined as

$$\bar{P} = \frac{P}{P_L}, \quad \bar{J} = \frac{J}{J_H} \in [0, 1]. \quad (14)$$

The corresponding derivatives are

$$\begin{aligned} \bar{P}_{,\bar{T}} &= \frac{P_{,T}}{P_L}(T_H - T_L), \\ \bar{P}_{,\bar{E}} &= \frac{E_0}{P_L}P_{,E}, \\ \bar{P}_{,\bar{T}\bar{T}} &= \frac{P_{,TT}}{P_L}(T_H - T_L)^2, \end{aligned} \quad (15)$$

and

$$\bar{J}_{,\bar{E}} = \frac{E_0}{J_H}J_{,E}, \quad \bar{J}_{,\bar{T}} = \frac{T_H - T_L}{J_H}J_{,T}. \quad (16)$$

Substituting Eqs. (13), (14), and (16) into Eqs. (9)–(11), we get the nondimensionalized governing equation

$$\frac{(\varepsilon_0 E_0 + P_L \bar{P}_{,\bar{E}})\ddot{\bar{E}}}{\tau^2} + \frac{\bar{C}_1}{\tau}\dot{\bar{E}} + \bar{C}_2 = 0, \quad (17)$$

where

$$\bar{C}_1 = \frac{\varepsilon_0 E_0 + P_L \bar{P}_{,\bar{E}}}{RC_{\text{ref}}} + \frac{dE_0}{AR} + J_H \bar{J}_{,\bar{E}}, \quad (18)$$

$$\begin{aligned} \bar{C}_2 &= \frac{P_L \bar{P}_{,\bar{T}}\ddot{\bar{T}} + P_L \bar{P}_{,\bar{T}\bar{T}}\dot{\bar{T}}^2}{\tau^2} \\ &+ \left(\frac{P_L \bar{P}_{,\bar{T}}}{\tau RC_{\text{ref}}} + \frac{J_H \bar{J}_{,\bar{T}}}{\tau}\right)\dot{\bar{T}} + \frac{J_H \bar{J}}{RC_{\text{ref}}}, \end{aligned} \quad (19)$$

which can be solved numerically under the initial conditions

$$\bar{E}(0) = 1, \quad \dot{\bar{E}}(0) = 0. \quad (20)$$

III. EXPERIMENT

We use three barium titanate-based ferroelectric materials to investigate the influence of electric leakage on pyroelectric energy conversion, and to verify our numerical model expressed by Eq. (17). These materials are polycrystalline BaTiO₃, Ba(Ti, Zr_{0.01})O₃ (BZT), and (Ba, Ca_{0.05})(Ti, Zr_{0.01}, Ce_{0.01})O₃ (tridoped BTO). The BTO and BZT are synthesized by a conventional ceramic sintering method; the detailed procedure is described in Ref. [6]. Their ferroelectric properties are summarized in Fig. 3(a). This shows that the addition of Zr increases the polarization in the ferroelectric phase. As shown in Figs. 2(b) and 3(b), the two materials exhibit similar trends in the leakage as the temperature increases under different electric fields. From the point of view of energy conversion, the figure of merit for BZT is higher than that for BTO, but the leakage is much smaller in BTO than in BZT. The elements Ca and Ce have been experimentally proven to be effective dopants for preventing electric leakage in barium titanate [19,20]. The mechanism is via a reduction in the number of oxygen vacancies, which consequently enhances the insulation [21,22]. The Ca dopant was found to narrow the temperature range of the phase transformation [19], which potentially improves the pyroelectric coefficient. Based on the BZT material, we design the tridoped BTO, which may give a small leakage while the pyroelectric performance is still maintained. The tridoped BTO is synthesized by the floating-zone method, which is commonly used for growing single crystals and textured polycrystals [23,24]. The addition of cerium to BTO may increase the grain size and change the photorefractive properties at high temperature [25,26], which facilitates the growth of crystals with

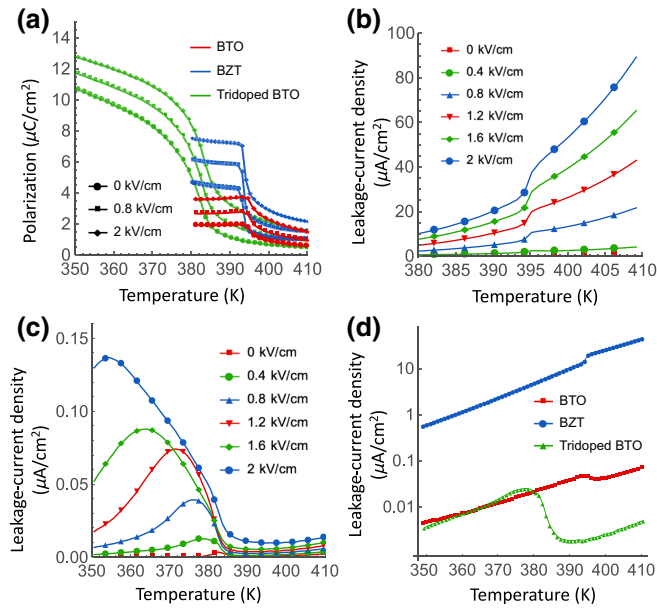


FIG. 3. (a) Temperature-dependent polarization of BTO (red), BZT (blue), and tridoped BTO (green), and temperature-dependent leakage-current density in (b) BZT and (c) tridoped BTO under electric fields from 0 to 2 kV/cm. (d) Comparison of leakage-current density among three capacitors made of BTO (red), BZT (blue), and tridoped BTO (green) under 30-V voltage.

a large grain size. In this study, we aim at synthesizing a pyroelectric material with better ferroelectric properties than those of BTO but with lower electric leakage than BZT to verify our thermodynamic model of pyroelectric energy conversion.

Powders of CaCO_3 (Alfa Aesar, 99.5%), CeO_2 (Alfa Aesar, 99.9%), ZrO_2 (Sigma Aldrich, 99%), BaCO_3 (Alfa Aesar, 99.8%), and TiO_2 (Alfa Aesar, 99.8%) are weighed out according to the stoichiometric formulation $\text{Ba}_{0.95}\text{Ca}_{0.05}\text{Ti}_{0.98}\text{Zr}_{0.01}\text{Ce}_{0.01}\text{O}_3$, dissolved in ethanol, and milled with zirconia balls in a planetary ball miller at 630 rpm for 24 h. The ball-milled solution is dried and calcined at 1000 °C for 10 h to obtain the tridoped barium titanate powder through solid-state reaction. Under 30 MPa hydrostatic pressure for 30 min, the powder is hot-pressed into a rod-shaped green body of diameter 6 mm and length 10 mm. The green body is sintered to form feed and seed rods in a four-mirror infrared furnace (Quantum Design IRF11-001-00) by passing it through the focal point slowly with an axial speed of 3 mm/h and an angular speed of 3 rpm. The feed and seed rods are aligned vertically for a floating-zone experiment using the same infrared furnace at a growth speed of 10 mm/h and a relative angular speed of 50 rpm in air. A molten zone is created and is monitored throughout the entire growth period. Finally, the as-grown rod is solidified and sliced along the growth direction. The composition of the as-grown bulk material is characterized by energy-dispersive x-ray-spectroscopy analysis.

The measured atomic composition is close to the nominal one to within 0.01 at. %.

The microstructures of our samples are characterized by use of a dual-beam-shear differential-interference-contrast microscope [27]. The surfaces of three samples are polished well with a 1- μm diamond suspension and etched with a 37% HCl solution for 10 min to reveal the grain morphology. Various crystallographic textures are distinguished by their brightness in the micrographs, since their reflectivity and phase contrast are different, as shown in Fig. 4. For BTO and BZT, the grain size is relatively fine, i.e., about 70 μm , while for the tridoped BTO, the grains grow about 5–8 times larger. The significant grain coarsening may be due to the floating-zone growth process [24]. Twinned structures are observed inside the grains for all three materials. Compared with the BTO and BZT samples made by the traditional synthesis approach, the tridoped BTO has many fewer pores. Consequently, it has the highest density, 5.774 g/cm^3 , compared with BTO (5.325 g/cm^3) and BZT (5.248 g/cm^3).

IV. RESULTS

Figure 3(a) compares the temperature-dependent polarization of BTO (red), BZT (blue), and tridoped BTO (green) under different electric fields from 0 to 2 kV/cm. Within the temperature range tested, all samples undergo a first-order phase transformation accompanied by an abrupt polarization jump from ferroelectric phase to paraelectric phase. Among these materials, the tridoped BTO exhibits the largest polarization (11 $\mu\text{C}/\text{cm}^2$) in the ferroelectric phase, making it a good candidate for pyroelectric energy conversion. In Fig. 3(c), the electric leakage is reduced greatly in tridoped BTO; its value is about 1/6 of that for BTO and 1/200 of that for BZT in the ferroelectric phase. The benchmark of the leakage-current density under the working conditions for energy conversion is shown in Fig. 3(d). In sharp contrast to BZT and BTO, the leakage in the tridoped ferroelectric material is much suppressed even in the temperature regime higher than the phase-transition temperature. In addition, we observe that the first-order phase transformation of tridoped BTO is more gradual than that of BZT, which indicates that the pyroelectric coefficient at the phase transformation is moderate compared with that of BZT. The measured pyroelectric coefficients are 0.42 $\mu\text{C}/\text{cm}^2 \text{K}$ for BTO, 1.89 $\mu\text{C}/\text{cm}^2 \text{K}$ for BZT, and 0.87 $\mu\text{C}/\text{cm}^2 \text{K}$ for tridoped BTO.

We use these three materials as dielectric layers to fabricate planar capacitors with geometries of 37.44 $\text{mm}^2 \times 0.74 \text{ mm}$ for BTO, 59.44 $\text{mm}^2 \times 0.257 \text{ mm}$ for BZT, and 66.59 $\text{mm}^2 \times 0.445 \text{ mm}$ for tridoped BTO. Using the energy-conversion electric circuit in Fig. 1(a), each of the phase-transforming capacitors is connected to a 100-k Ω load resistor and a 50- μF reference capacitor in series. Before energy conversion, we use an external dc

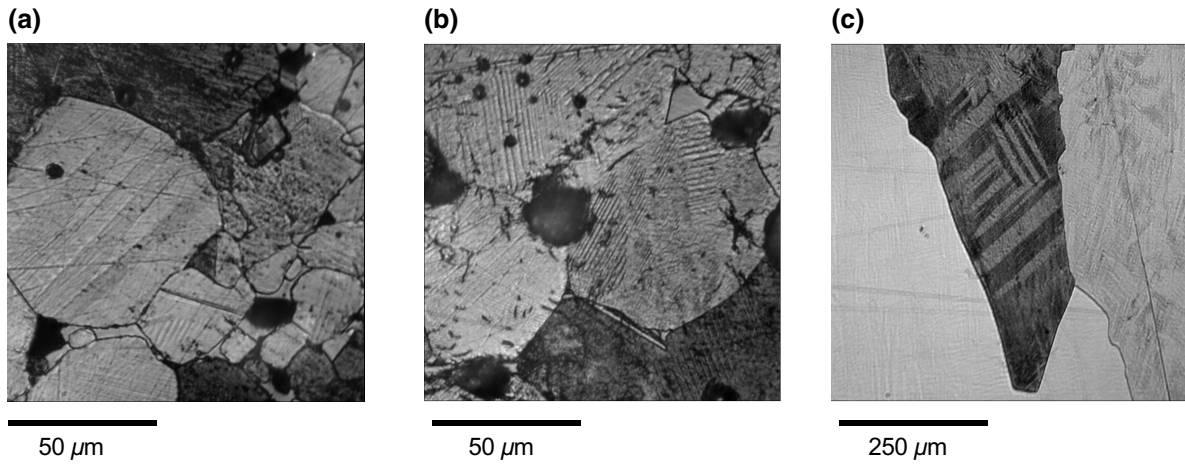


FIG. 4. Micrographs of grain morphology for (a) BTO, (b) BZT, and (c) tridoped BTO obtained with a dual-beam-shear differential-interference-contrast microscope.

voltage source (Tektronix PS280) to charge the entire system so that both the phase-transforming capacitor and the reference capacitor are at a voltage of 30 V, and no electric charge flows in the circuit. Then, the external dc voltage source is disconnected at a temperature $T_L < T_c$. During the demonstration of pyroelectric energy conversion, the phase transformation is induced by passing the material through the transformation temperature under an electric field. The ferroelectric phase is polarized by the applied electric field at low temperature. The temperature-dependent polarization follows the constitutive relation in Fig. 3(a) with application of the external field.

We use a custom-made thermal stage to drive the temperature of the phase-transforming capacitor in a periodic pattern around its transition temperature. For each of the phase-transforming capacitors, we collect five consecutive thermal cycles, as shown in Figs. 5(a), 5(c), and 5(e), corresponding to $T_L = 360$ K and $T_H = 410$ K. The total durations of all thermal cycles are 175 s for BTO, 133 s for BZT, and 120 s for tridoped BTO; these values are used to derive the nondimensionalized time variable. The average transformation times per cycle for them, that is, the value of τ in Eq. (13), are calculated as 17.5 s for BTO, 13.3 s for BZT, and 12 s for tridoped BTO. The normalized

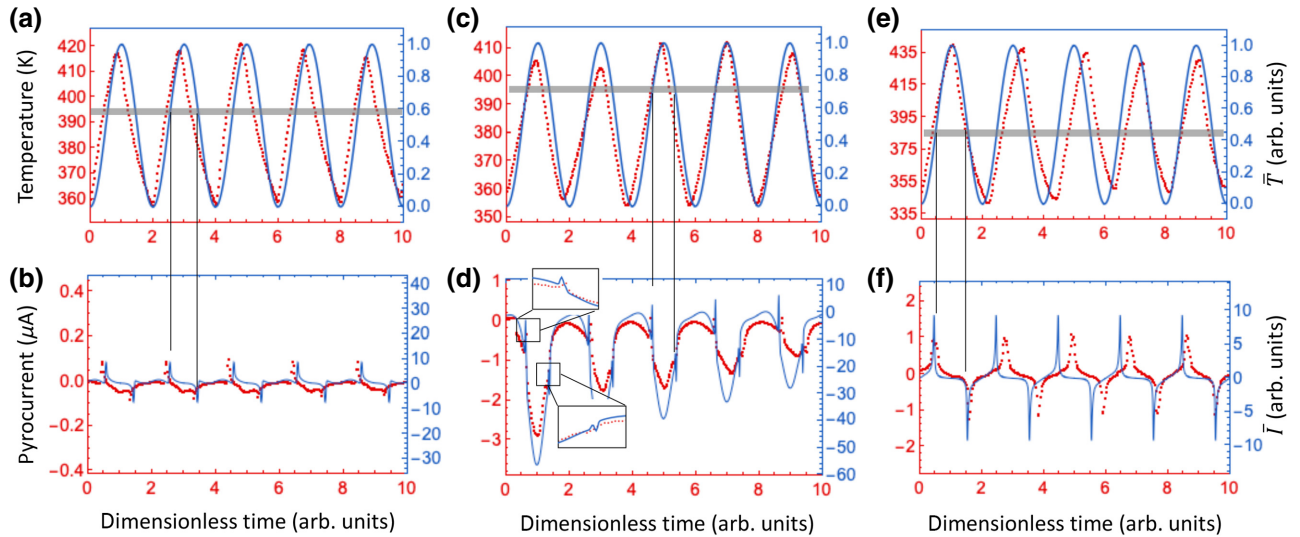


FIG. 5. Measured and simulated pyroelectric energy conversion by use of temperature fluctuations in (a) BTO, (c) BZT, and (e) tridoped BTO, corresponding to the pyrocurrents in (b) BTO, (d) BZT, and (f) tridoped BTO. The experimental results are represented in red, while the simulated results are plotted in blue.

temperature patterns for these materials are plotted as blue curves in Figs. 5(a), 5(c), and 5(e).

The pyrocurrent is characterized by the current passing through the load resistor, of resistance R , calculated as

$$I_p = i_p A, \quad (21)$$

where

$$i_p = -(\dot{q} + J) = -[(\epsilon_0 + P_{,E})\dot{E} + P_{,T}\dot{T} + J] \quad (22)$$

is the pyrocurrent density for an area A . This current is attributed to a charge flow driven by the change in polarization and the internal leakage in the pyroelectric capacitor. As a result, the electric field across the pyroelectric capacitor decreases continuously throughout the energy-conversion process. The pyrocurrent measured in the experiments (red) is shown in Figs. 5(b) for BTO, 5(d) for BZT, and 5(f) for tridoped BTO, corresponding to numerical solutions (blue) of Eq. (17). The generation of a pyrocurrent in consecutive thermal cycles is well captured by our thermodynamic model for the three samples with different ferroelectric properties. We conjecture that three factors play an important role in pyroelectric energy conversion by use of a first-order phase transformation: (1) the polarization jump between the states before and after the phase transformation, (2) the pyroelectric coefficient at the transition temperature, and (3) the leakage-current density within the range of thermal fluctuations applied to the sample. For the BTO sample, all three factors are low, which indicates that it is a good insulator but a bad pyroelectric-conversion material, corresponding to a very small pyrocurrent density (66.8 nA/cm^2) in all five cycles. The BZT sample is a good energy-conversion material, having the largest pyroelectric coefficient among the three samples, and enhanced polarization in the ferroelectric phase. But it is a bad insulator, with a non-negligible leakage. Considering a full loop of the phase transformation, its averaged pyrocurrent density for the first cycle is $1.17 \text{ }\mu\text{A/cm}^2$, which degrades to $0.34 \text{ }\mu\text{A/cm}^2$ after five cycles. Since the charge leakage is unidirectional, both the measured and the computed pyrocurrent for BZT are biased toward the negative direction with respect to the neutral point. The contribution of the leakage current to the work done in the load resistor sometimes hides the true amount of electric energy converted by the pyroelectric material [28–30]. For the tridoped BTO, both the pyroelectric capability and the insulation are enhanced greatly. As a result, it shows a pyrocurrent density of $1.95 \text{ }\mu\text{A/cm}^2$ without degradation at the end of the fifth cycle. The pyrocurrent achieved in tridoped BTO is around 3 times larger than the largest pyrocurrent reported so far for single-crystal barium titanate with a narrow transition window (5 K) when the polar axis is aligned with the electric field [7].

V. DISCUSSION

We use the least leaky pyroelectric capacitor (i.e., the tridoped-BTO capacitor) to conduct more cycles under different working conditions. Figure 6 compares the pyrocurrent given by the tridoped BTO capacitor in a fully discharged state and a 30-V charged state. In the same experiment setup as used for energy conversion, the generated pyrocurrent strongly depends on the initial state $Q_L(V_L, T_L)$. A fully discharged pyroelectric capacitor with $V_L = 0$ produces a much smaller amount of electricity than that produced by the same capacitor with $V_L = 30 \text{ V}$. If the pyroelectric material is leaky, the capacitor continues to discharge while converting energy cyclically. This intrinsic discharging eventually causes the production of electricity in the system to cease, even though the material itself is pyroelectrically functional.

This opens up a discussion of the effective life of a pyroelectric energy converter with intrinsic leakage. Let τ denote the duration of the thermodynamic half cycle from (P_L, E_L, T_L) to (P_H, E_H, T_H) , where the temperature range

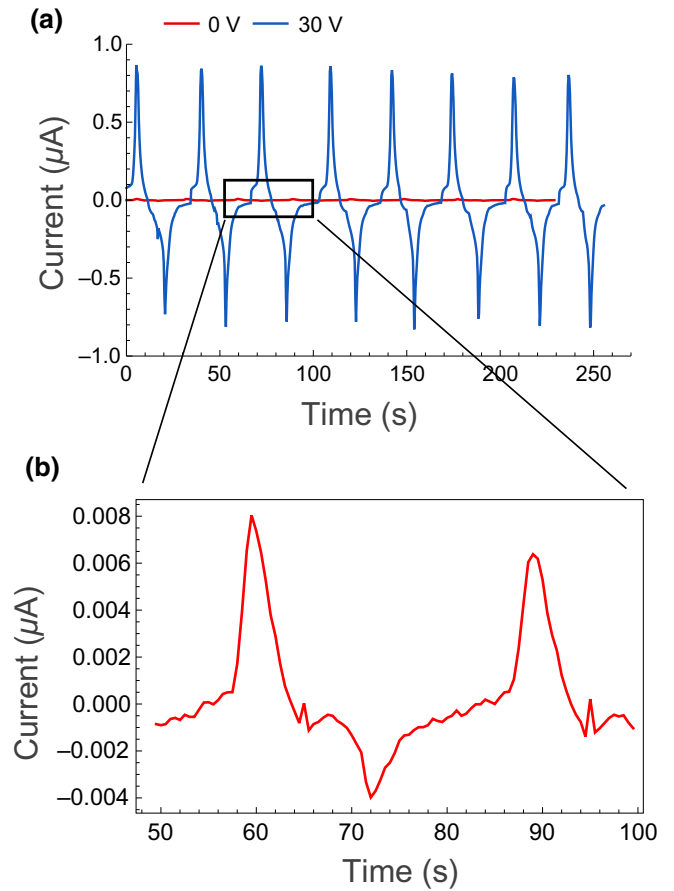


FIG. 6. (a) Measured current generated by tridoped BTO under zero electric field (red) and positive electric field $E > 0$ corresponding to 30-V capacitor voltage. (b) Enlarged region of the measured current under zero electric field.

TABLE I. Performance of pyroelectric energy converters over their effective life, where W is the total output electric energy density, and W_π is the total pyrowork.

Material	N^*	$W(N^*)$ (J/cm ³)	$W_\pi(N^*)$ (J/cm ³)	$\frac{W(N^*)}{W_\pi(N^*)}$ (%)
BTO	502	6.24×10^{-4}	8.36×10^{-4}	75
BZT	9	8.92×10^{-4}	0.0049	18
Tridoped BTO	1389	0.1997	0.2018	99

$[T_L, T_H]$ fully covers the first-order phase transformation from ferroelectric to paraelectric. We assume that the cooling process from T_H is time-symmetric with respect to the first thermodynamic half cycle. Then the electric field in the N th thermodynamic cycle is

$$E(2N\tau) < \dots < E(2\tau) < E(0) = \frac{V_0}{d}. \quad (23)$$

By solving Eq. (17), we can calculate the electric field $E(2N\tau)$ for $N \in \mathbb{Z}^+$. The effective life is defined as the number of thermodynamic cycles N^* such that

$$E(2(N^* + 1)\tau) < \frac{V_0}{2d} < E(2N^*\tau). \quad (24)$$

This means that after N^* cycles, the electric field in the pyroelectric capacitor has been reduced to half of the value that it had when the capacitor was initially charged. If we consider only the current output from pyroelectric energy conversion, the output electric energy density in the load resistor can be calculated as

$$W(N) = \frac{AR}{d} \int_0^{2N\tau} \dot{q}^2 dt, \quad (25)$$

where \dot{q} denotes the current density passing through the load resistor R . Considering the work done by the electrostatic force in the pyroelectric capacitor during the cyclic thermodynamic processes, we define the pyrowork as

$$W_\pi(N) = - \int_0^{2N\tau} E \dot{P} dt. \quad (26)$$

Here the electric field should satisfy the governing equation (17) for the driving temperature profile $T(t)$. The polarization is evaluated by use of the experimentally characterized constitutive relations (Figs. 2 and 3). We calculate the effective life, the output work density, and the pyrowork density for BTO, BZT, and tridoped BTO capacitors; the results are summarized in Table I.

Without leakage, the output electric energy is expected to be the same as the electrostatic energy produced by the pyroelectric capacitor [6]. The loss of energy captured by our thermodynamic model is due to the internal loss of charge during cyclic energy-conversion processes. For

the most leaky capacitor, made from BZT, the pyroelectric energy conversion ceases at the end of the ninth cycle. Until it is recharged by an external battery, it will not then produce electricity by the pyroelectric effect even if the pyroelectric material is still functional. Overall, the BZT capacitor outputs 8.92×10^{-4} J/cm³ of electric energy converted purely from heat. For the BTO-based capacitors, the energy-conversion performance does not degrade much over hundreds to thousands of cycles. Particularly, the Ce-, Ca-, and Zr-doped BTO capacitor generates 0.2 J/cm³ of electric energy in a total of 1389 cycles, that is, 3 orders of magnitude larger than the amount of energy produced by the other two materials. More importantly, the electric energy collected in the external circuit is almost equal to the electrostatic work done during the pyroelectric energy conversion. With such a value, a pyroelectric device can be actually useful in real energy applications.

VI. CONCLUSION

This paper underlines the influence of leakage on the performance of pyroelectric energy conversion using first-order phase-transforming ferroelectrics. Through experiments and numerical simulations done for BTO, BZT, and tridoped BTO, we show that tridoped BTO is the most suitable material for pyroelectric energy conversion because of its singular polarization properties and much reduced leakage. Our model confirms that the degradation of the energy-conversion performance strongly depends on the leakage-current density of the pyroelectric material. To design a power-source-free pyroelectric energy-conversion system that can continuously harvest electricity from waste heat, both the pyroelectric properties and the leakage-current density need to be taken into account. Our work should provide a useful reference for the future development of high-performance ferroelectric materials and the design of energy-conversion systems.

ACKNOWLEDGMENTS

C.Z. and X.C. are grateful for financial support from the HK Research Grants Council under Grants No. 16201118 and No. 16201019 and the Bridge Gap Fund, Grant No. BGF.009.19/20, from the HKUST Technology Transfer Center.

- [1] S. I. Garcia, R. F. Garcia, J. C. Carril, and D. I. Garcia, A review of thermodynamic cycles used in low temperature recovery systems over the last two years, *Renewable Sustainable Energy Rev.* **81**, 760 (2018).
- [2] R. B. Olsen, D. A. Bruno, and J. M. Briscoe, Pyroelectric conversion cycles, *J. Appl. Phys.* **58**, 4709 (1985).
- [3] G. Sebald, D. Guyomar, and A. Agbossou, On thermoelectric and pyroelectric energy harvesting, *Smart Mater. Struct.* **18**, 125006 (2009).
- [4] Y. Yang, W. Guo, K. C. Pradel, G. Zhu, Y. Zhou, Y. Zhang, Y. Hu, L. Lin, and Z. L. Wang, Pyroelectric nanogenerators for harvesting thermoelectric energy, *Nano Lett.* **12**, 2833 (2012).
- [5] S. Pandya, J. Wilbur, J. Kim, R. Gao, A. Dasgupta, C. Dames, and L. W. Martin, Pyroelectric energy conversion with large energy and power density in relaxor ferroelectric thin films, *Nat. Mater.* **17**, 432 (2018).
- [6] C. Zhang, Y. Song, M. Wegner, E. Quandt, and X. Chen, Power-Source-Free Analysis of Pyroelectric Energy Conversion, *Phys. Rev. Appl.* **12**, 014063 (2019).
- [7] A. Bucsek, W. Nunn, B. Jalan, and R. D. James, Direct Conversion of Heat to Electricity Using First-Order Phase Transformations in Ferroelectrics, *Phys. Rev. Appl.* **12**, 034043 (2019).
- [8] A. N. Bucsek, W. Nunn, B. Jalan, and R. D. James, Energy conversion by phase transformation in the small-temperature-difference regime, *Annu. Rev. Mater. Res.* **50**, 283 (2020).
- [9] B. Nagaraj, S. Aggarwal, T. Song, T. Sawhney, and R. Ramesh, Leakage current mechanisms in lead-based thin-film ferroelectric capacitors, *Phys. Rev. B* **59**, 16022 (1999).
- [10] G. W. Pabst, L. W. Martin, Y.-H. Chu, and R. Ramesh, Leakage mechanisms in BiFeO₃ thin films, *Appl. Phys. Lett.* **90**, 072902 (2007).
- [11] L. Pintilie, I. Vrejoiu, D. Hesse, G. LeRhun, and M. Alexe, Ferroelectric polarization-leakage current relation in high quality epitaxial Pb(Zr, Ti)O₃ films, *Phys. Rev. B* **75**, 104103 (2007).
- [12] H. Yang, M. Jain, N. Suvorova, H. Zhou, H. Luo, D. Feldmann, P. Dowden, R. DePaula, S. Foltyn, and Q. Jia, Temperature-dependent leakage mechanisms of Pt/BiFeO₃/SrRuO₃ thin film capacitors, *Appl. Phys. Lett.* **91**, 072911 (2007).
- [13] W. Sun, Z. Zhou, J. Luo, K. Wang, and J.-F. Li, Leakage current characteristics and Sm/Ti doping effect in BiFeO₃ thin films on silicon wafers, *J. Appl. Phys.* **121**, 064101 (2017).
- [14] Q. Ke, X. Lou, Y. Wang, and J. Wang, Oxygen-vacancy-related relaxation and scaling behaviors of Bi_{0.9}La_{0.1}Fe_{0.98}Mg_{0.02}O₃ ferroelectric thin films, *Phys. Rev. B* **82**, 024102 (2010).
- [15] A. K. Bain and P. Chand, *Ferroelectrics: Principles and Applications* (John Wiley & Sons, Weinheim, Germany, 2017).
- [16] C. R. Bowen, J. Taylor, E. LeBoulbar, D. Zabek, A. Chauhan, and R. Vaish, Pyroelectric materials and devices for energy harvesting applications, *Energy Environ. Sci.* **7**, 3836 (2014).
- [17] B. He and Z. Wang, Enhancement of the electrical properties in BaTiO₃/PbZr_{0.52}Ti_{0.48}O₃ ferroelectric superlattices, *ACS Appl. Mater. Interfaces* **8**, 6736 (2016).
- [18] S. Hajra, P. Sharma, S. Sahoo, P. Rout, and R. Choudhary, Processing and electrical properties of gallium-substituted lead zirconate titanate ceramics, *Appl. Phys. A* **123**, 1 (2017).
- [19] A. E.-R. Mahmoud, M. Ezzeldien, and S. Parashar, Enhancement of switching/un-switching leakage current and ferroelectric properties appraised by pumd method of (Ba_{1-x}Ca_x)TiO₃ lead free piezoelectric near MPB, *Solid State Sci.* **93**, 44 (2019).
- [20] S. Wang, B. Cheng, C. Wang, S. Redfern, S. Dai, K. Jin, H. Lu, Y. Zhou, Z. Chen, and G. Yang, Influence of Ce doping on leakage current in Ba_{0.5}Sr_{0.5}TiO₃ films, *J. Phys. D: Appl. Phys.* **38**, 2253 (2005).
- [21] J. Scott, Ferroelectrics go bananas, *J. Phys.: Condens. Matter* **20**, 021001 (2007).
- [22] Y. Sakabe, N. Wada, T. Hiramatsu, and T. Tonogaki, Dielectric properties of fine-grained BaTiO₃ ceramics doped with CaO, *Jpn. J. Appl. Phys.* **41**, 6922 (2002).
- [23] H. Kojima, M. Watanabe, and I. Tanaka, Crystal growth of strontium-substituted barium titanate (Ba_{1-x}Sr_xTiO₃) by the floating zone method, *J. Cryst Growth* **155**, 70 (1995).
- [24] F. Brown and W. Todt, Floating-zone BaTiO₃: Preparation and properties, *J. Appl. Phys.* **35**, 1594 (1964).
- [25] S. Dou, Y. Ding, H. J. Eichler, Y. Zhu, and P. Ye, Temperature dependent photorefractive properties of a Ce-doped BaTiO₃ crystal, *Opt. Commun.* **131**, 322 (1996).
- [26] S. Yasmm, S. Choudhury, M. Hakim, A. Bhuiyan, and M. Rahman, Effect of cerium doping on microstructure and dielectric properties of BaTiO₃ ceramics, *J. Mater. Sci. Technol.* **27**, 759 (2011).
- [27] Z. Zeng, H.-C. Chiu, L. Zhao, T. Zhao, C. Zhang, M. Karami, H. Yu, S. Du, and X. Chen, Dual beam-shear differential interference microscopy for full-field surface deformation gradient characterization, *J. Mech. Phys. Solids* **145**, 104162 (2020).
- [28] S. Smith, A. Kitahara, M. Rodriguez, M. Henry, M. Brumbach, and J. Ihlefeld, Pyroelectric response in crystalline hafnium zirconium oxide (Hf_{1-x}Zr_xO₂) thin films, *Appl. Phys. Lett.* **110**, 072901 (2017).
- [29] M.-H. You, X.-X. Wang, X. Yan, J. Zhang, W.-Z. Song, M. Yu, Z.-Y. Fan, S. Ramakrishna, and Y.-Z. Long, A self-powered flexible hybrid piezoelectric-pyroelectric nanogenerator based on non-woven nanofiber membranes, *J. Mater. Chem. A* **6**, 3500 (2018).
- [30] K. Mistewicz, M. Jesionek, M. Nowak, and M. Kozioł, SbSeI pyroelectric nanogenerator for a low temperature waste heat recovery, *Nano Energy* **64**, 103906 (2019).